Why do we like dyons!?

V.G.Bornyakov, E.-M.Ilgenfritz, B.V.Martemyanov

Content:

1. What are dyons?
2. Who are we?
3. Observation of dyons in SU(2) LGT (cooling, smearing, low modes filtering)
4. Observation of dyons in SU(3) LGT (cooling, low modes filtering)
5. Observation of dyons in lattice QCD (low modes filtering)

Gauge topology: from lattice to colliders. ECT* workshop, November, 7 - 11, 2016

What are dyons?

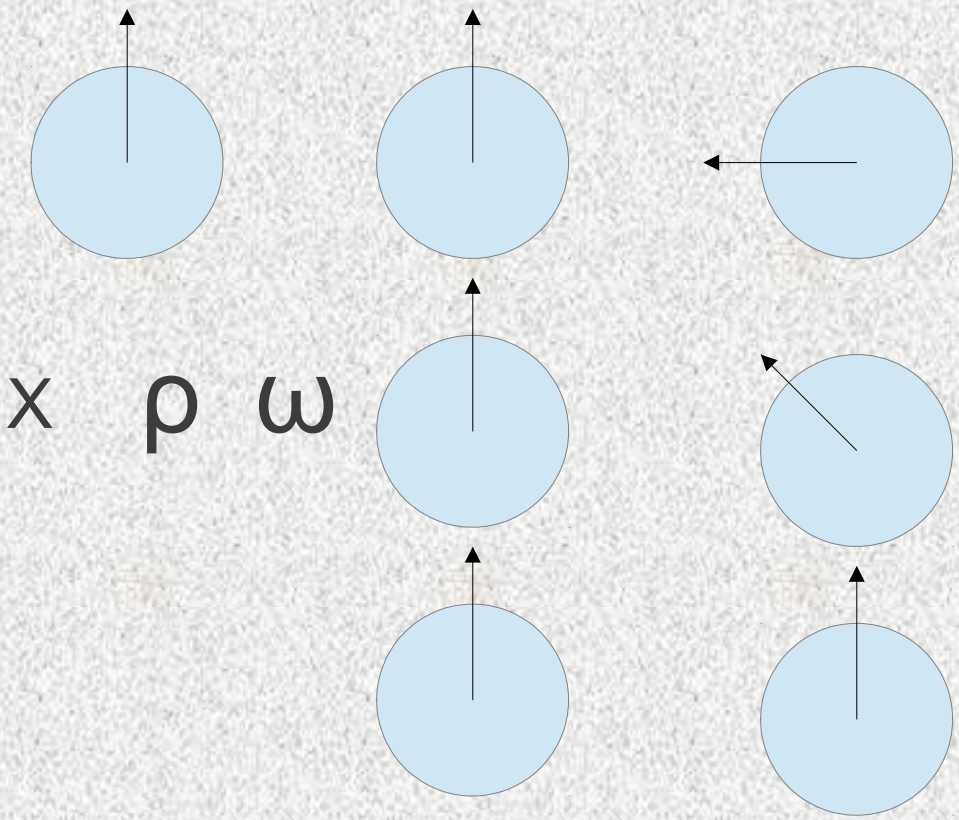

x ρ ω

+ b + φ = 2πv

SU(2)

$d = \pi\rho^2/b$

m1:m2 = v :(1-v)

PL = cos(πv)

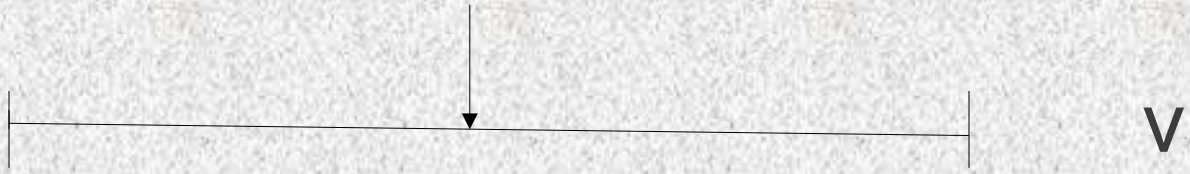

Dyons are magnetic monopoles

PL(dyons) = +1,-1

Zero modes of Dirac operator - on dyons

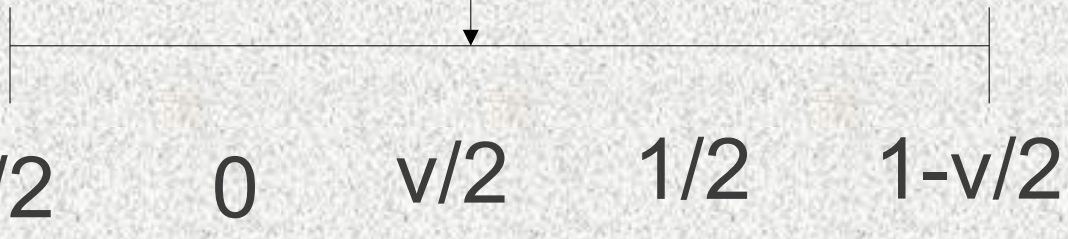

SU(3)

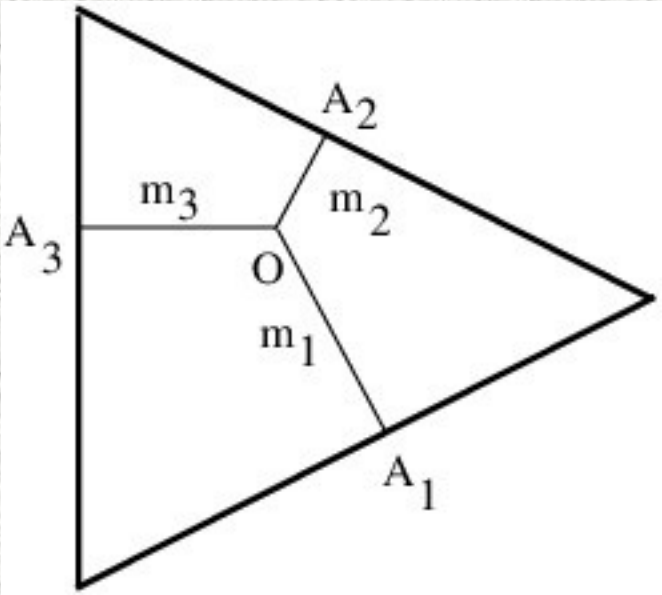

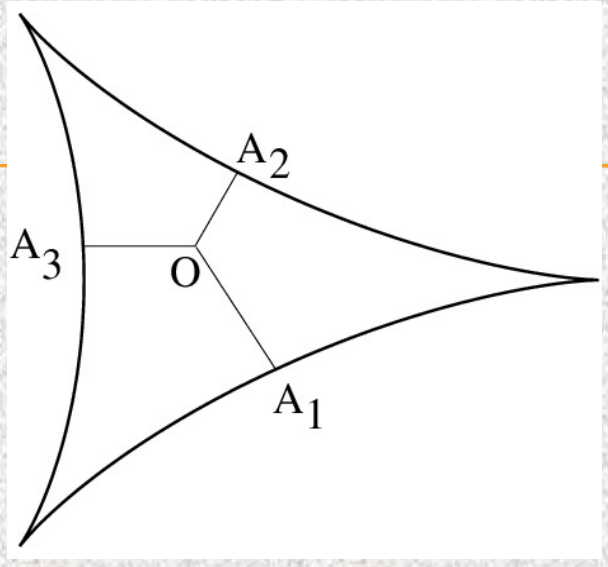

$$\begin{pmatrix} \exp(i2\pi\mu_1) & & \\ & \exp(i2\pi\mu_2) & \\ & & \exp(i2\pi\mu_3) \end{pmatrix} =$$

$$m_1=\mu_2-\mu_1$$
$$m_2=\mu_3-\mu_2$$
$$m_3=1+\mu_1-\mu_3$$

μ_1 μ_2 μ_3 $1+\mu_1$

$$\mu_1+\mu_2+\mu_3=0$$

Who are we?

Yu.A.Simonov et al. 1995

Pierre van Baal et al. 1998

M. Mueller-Preussker et al. 2000

Falk Bruckmann et al. 2002

D.I. Diakonov et al. 2004

M. Unsal et al. 2009

E. Shuryak et al. 2012

Observation of dyons in SU(2) LGT

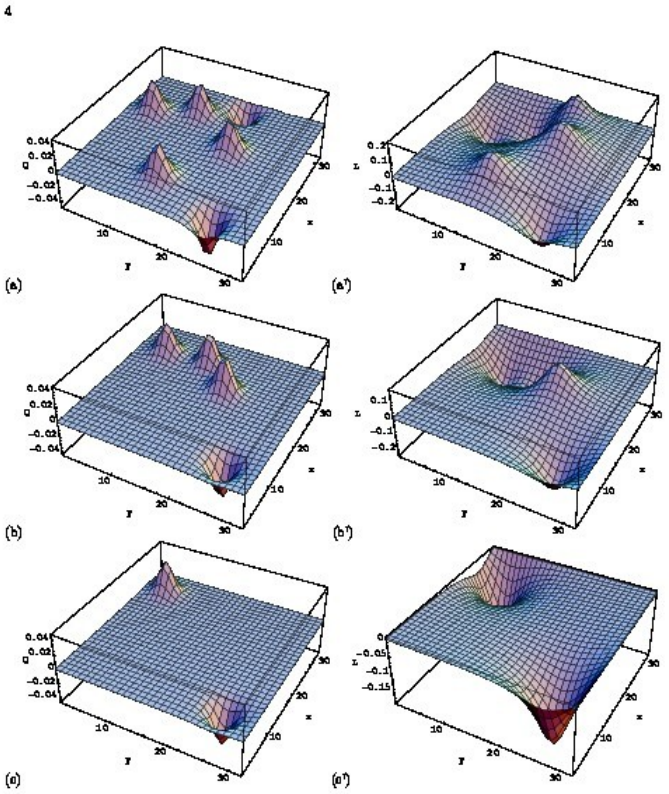

Figure 1. Topological charge density (a, b, c) and corresponding spatial Polyakov line distribution (a', b', c') at different cooling stages for a typical gauge field configuration. The transition (a, a') → (b, b') shows the annihilation of a $D\bar{D}$ pair and (b, b') → (c, c') the annihilation of a $D\bar{D}$ pair, respectively.

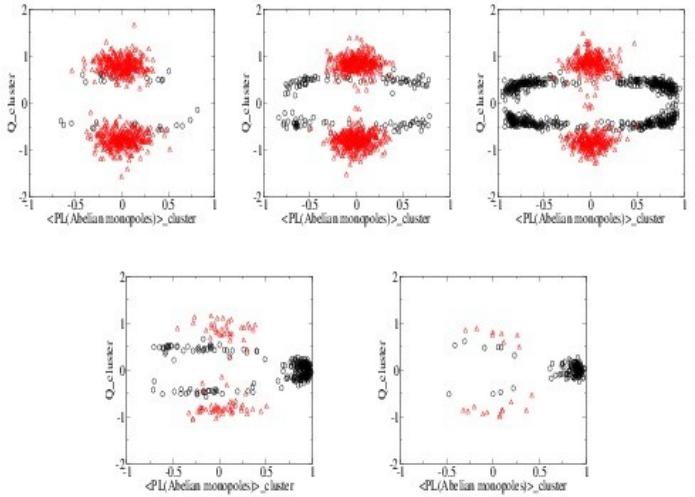

FIG. 5: (color online) Scatter plots in the $\{Q_{cluster}, \langle PL(\text{Abelian monopoles})\rangle_{cluster}\}$ plane for $\beta = 2.2$, 2.3, 2.4 (upper row from left to right, confinement) and for $\beta = 2.5$, 2.6 (lower row from left to right, deconfinement). The circles represent dyon clusters, the triangles antidyon clusters.

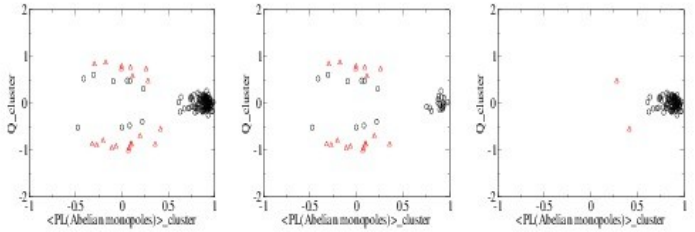

FIG. 6: (color online) Scatter plots in the $\{Q_{cluster}, \langle PL(\text{Abelian monopoles})\rangle_{cluster}\}$ plane for $\beta = 2.6$. The left figure is the sum of the other two. The figure in the center shows configurations (45 from 200 configurations) with topological charge $|Q| = 1$ ($0.5 \leq |Q| \leq 1.5$), the right figure the complementary 155 configurations with zero topological charge $Q = 0$ ($|Q| \leq 0.5$). The meaning of the symbols is the same as in Fig. 5.

skeleton, denoted as $\{PL(\text{Abelian monopoles})\}_{cluster}$. The points in these scatter plots represent cluster that have been identified in one or the other way. As it can be seen from this figure, in the confined

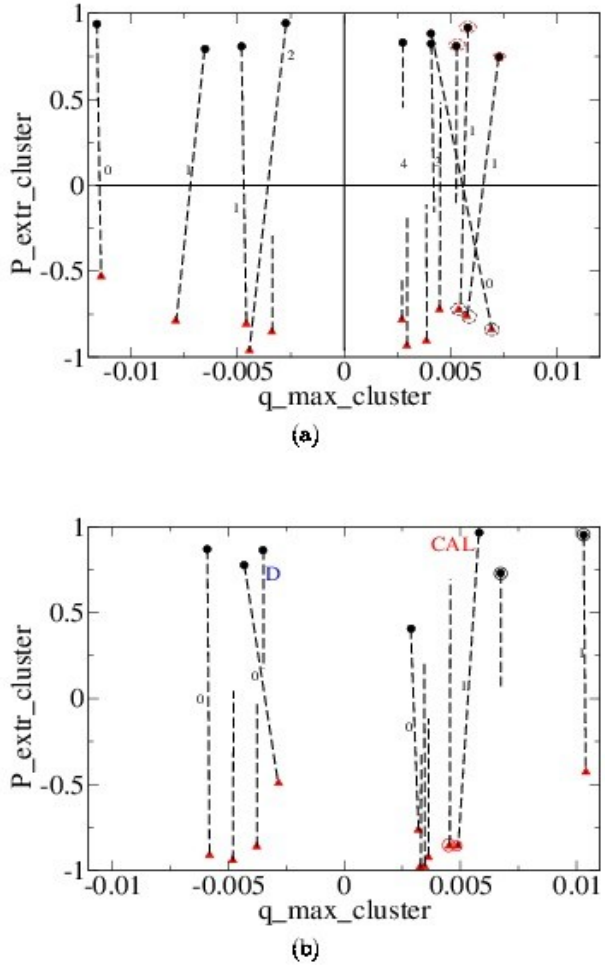

FIG. 5: The maxima of clusters of the fermionic $|q(n)|$ seen under periodic boundary condition (filled circles) and under antiperiodic boundary condition (filled triangles) for two configurations (a) and (b) in the sample, shown in the ($q_{\max\ \mathrm{cluster}}$, $P_{\mathrm{extr\ cluster}}$) plane (the precise meaning is explained in the text). Peaks at opposite-sign of $P_{\mathrm{extr\ cluster}}$, that are connected by dashed lines, have appeared under different boundary conditions at the same space-time position ("not jumping") and are interpreted as calorons. Isolated peaks have appeared only once under the respective boundary condition at the given position ("jumping") and are interpreted as dyons. The marked objects "D" and "CAL" in (b) are portrayed in detail in Fig. 6.

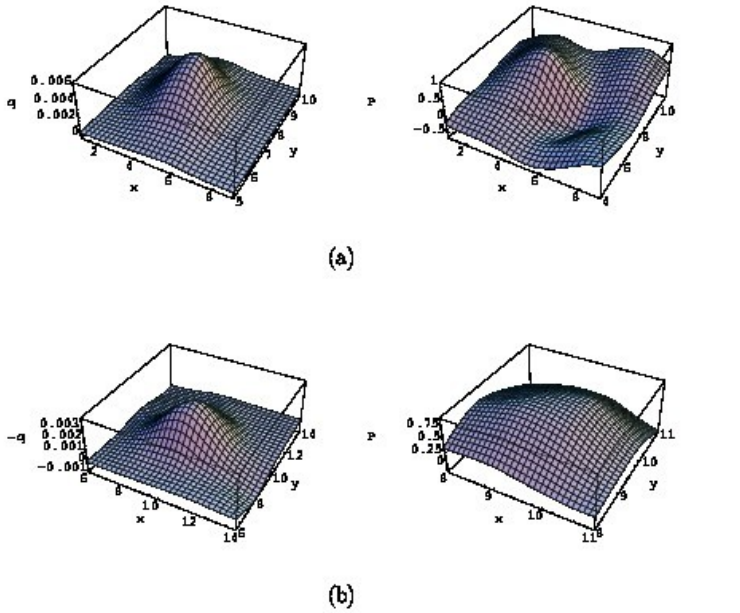

FIG. 6: The fermionic topological charge density $q^{(n/a)}(n)$ (left) and the Polyakov loop $p(\vec{n})$ (right): (a) for a typical caloron cluster (when $q^{(0)}(n) \approx q^{(a)}(n)$) and (b) for a typical dyon cluster (which was visible only in $q^{(p)}(n)$) from Fig. 5 (b). The topological density and the Polyakov loop are represented as function over part of the (x, y)-plane. Please notice the different scales for the topological charge density and for the Polyakov loop. The Polyakov loop is measured after $N_{\mathrm{APE}} = 10$ smearing steps.

Observation of dyons in SU(3) LGT

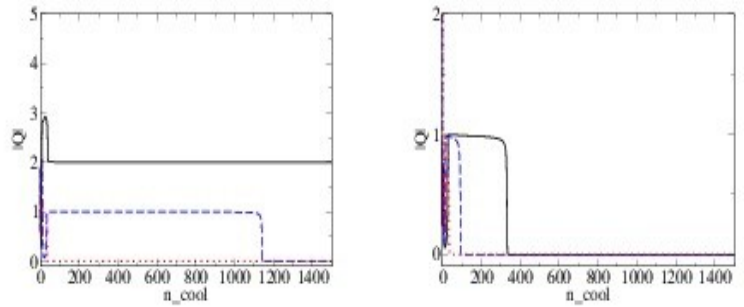

FIG. 1: Cooling histories of $|Q|$ corresponding to $\varepsilon = 1$ (Wilson action, red dotted lines), $\varepsilon = 0$ (slightly overimproved action, blue dashed lines) and $\varepsilon = -1$ (overimproved action as used in the rest of this paper, black solid lines). Left: different cooling histories for one configuration from the confined phase. Right: different cooling histories for a (conditionally stable) caloron in a configuration taken from the transition region.

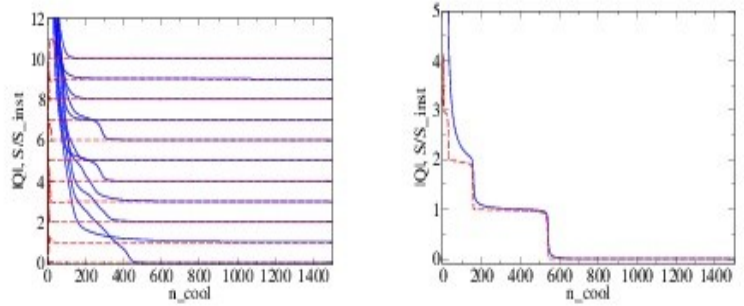

FIG. 2: Typical cooling histories of configurations from the confined phase (left). The cooling history of an (finally unstable) caloron in a configuration taken from the transition region (right). The red dashed lines represent $|Q|$, the blue solid lines represent S.

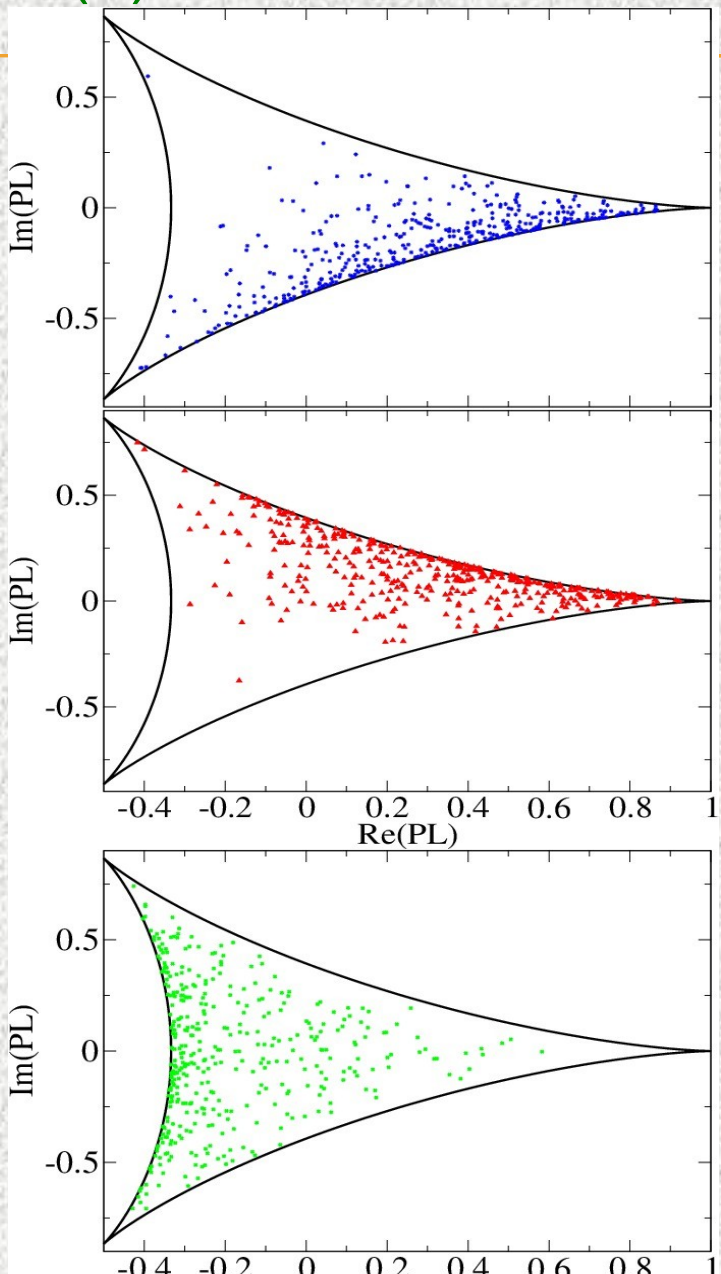

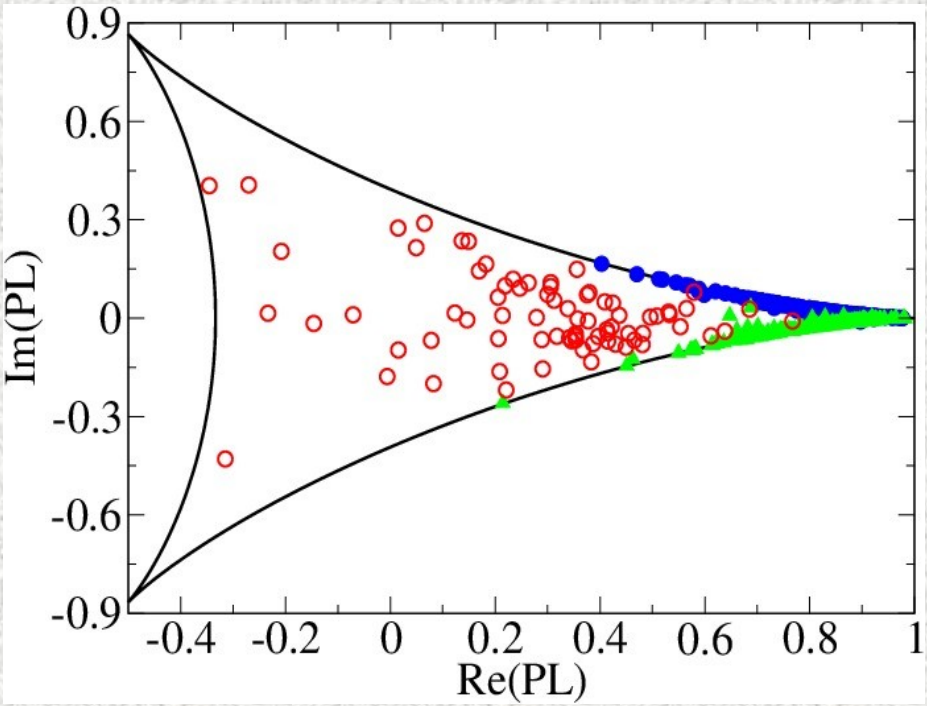
0.9
0.6
0.3
0
-0.3
-0.6
-0.9
Im(PL)
-0.4
-0.2
0
0.2
0.4
0.6
0.8
1
Re(PL)

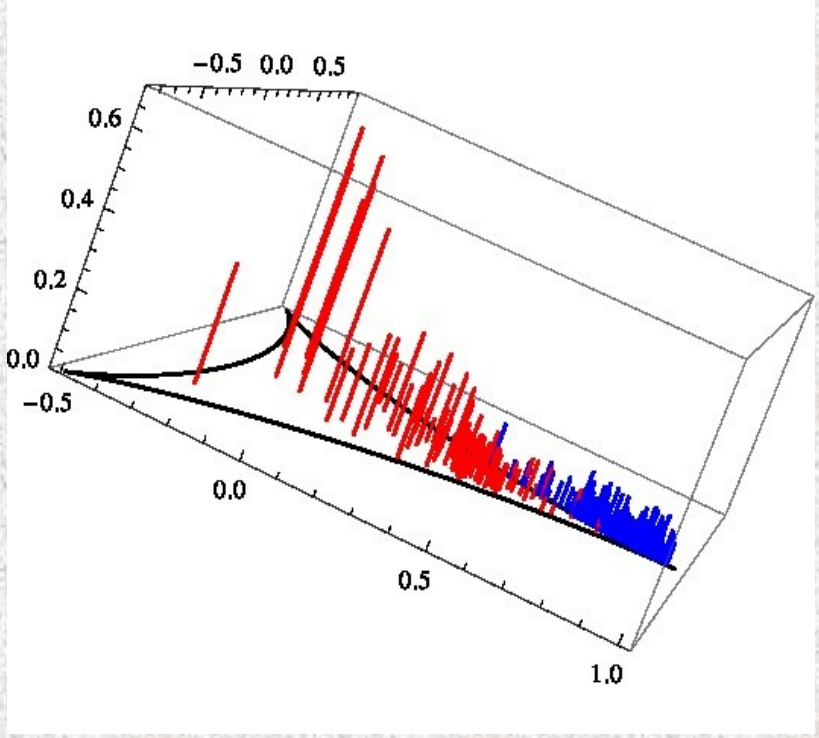
−0.5 0.0 0.5
0.6
0.4
0.2
0.0
−0.5
0.0
0.5
1.0

Observation of dyons in LQCD

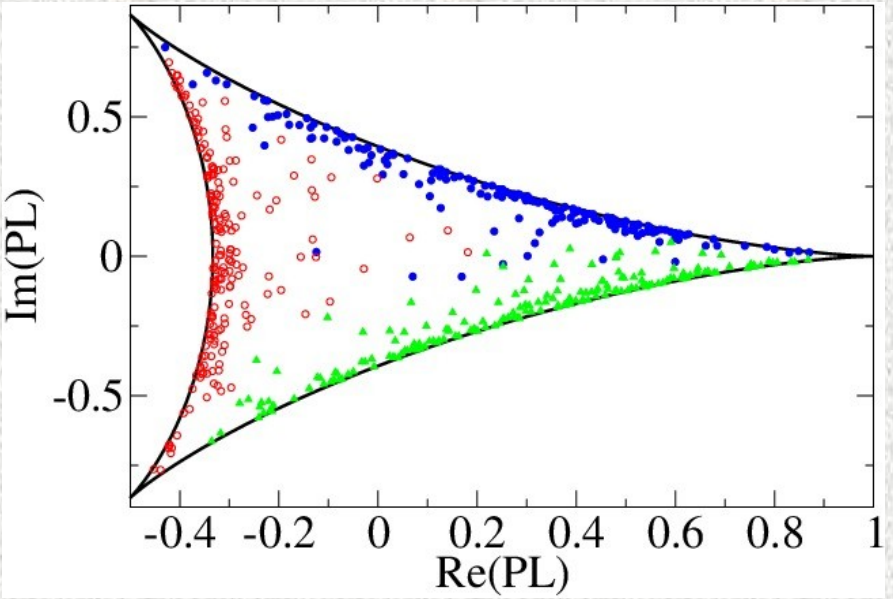

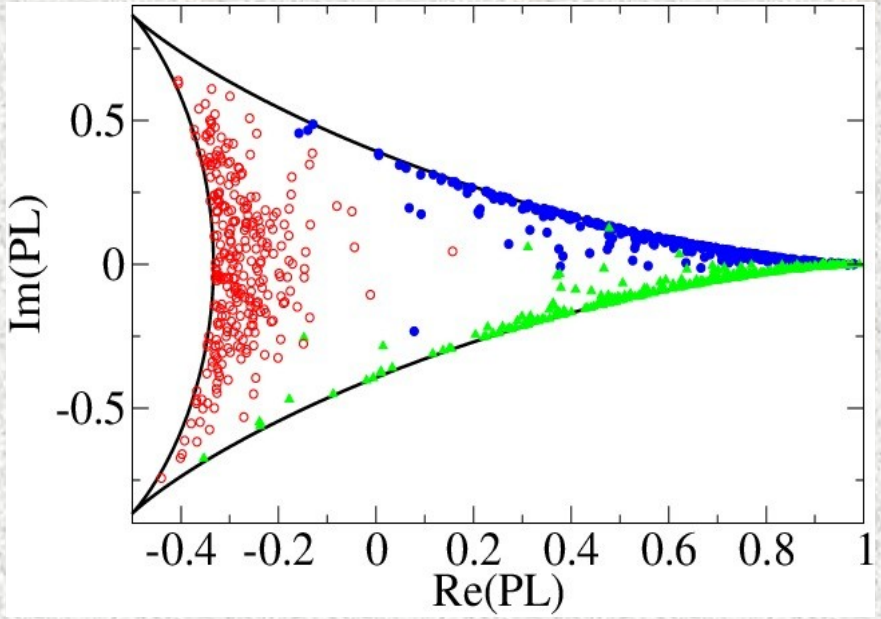

Conclusion

1. Instanton mechanism is able to explain chiral symmetry breaking while it fails to provide a mechanism for confinement.
2. Constituent dyons of Kraan-van Baal-Lee-Lu calorons give some room to reproduce certain features of confinement.
3. That is why it is interesting and important to find and investigate them in lattice simulations of gauge fields.
4. These investigations show the presence of dyons in thermal lattice gauge fields.
5. Quantitative knowledge of characteristics of dyon ensembles in these fields could be the next step of investigations.